Heliyon 10 (2024) e35969

Contents lists available at ScienceDirect

Heliyon

journal homepage: www.cell.com/heliyon

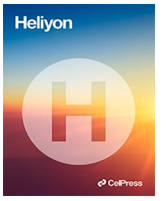

Research article

Enhanced lithium host performance of multi-walled carbon nanotubes through acidic functionalization for lithium–sulfur batteries

Gwang-Hun Kim [1], Asif Raza [1], You-Jin Lee, Doohun Kim, Jun-Woo Park [**], Hae-Young Choi [*]

Next-Generation Battery Research Center, Korea Electrotechnology Research Institute, Changwon, 51543, South Korea

ARTICLE INFO

Keywords:
Lithium-sulfur battery
Functionalized MWCNT
Sulfur content
Slurry dispersion
Acidic treatment

ABSTRACT

Carbon nanotubes (CNTs) have been explored as a potential cathode material for lithium-sulfur (Li–S) batteries owing to their unique structure. However, traditional CNTs exhibit poor dispersion properties when preparing electrodes. The non-uniform distribution of the conductive agents hinders the formation of enough sites for sulfur loading, which results in the aggregation of sulfur/Li_2S and severe polarization. In this study, we propose the acidic functionalization of CNTs in the cathode structure as a practical solution for mitigating the poor dispersion and polysulfide shuttling in lithium-sulfur batteries. Multiwalled CNTs were functionalized by oxidation through acidic treatment using sulfuric, nitric, and mixed acids. The cathode prepared with a mixture of sulfuric and nitric acids showed a coulombic efficiency of 99 % after 100 cycles, with a discharge capacity of 743 mAh g^{-1}. These findings demonstrate the effectiveness of the acidic functionalization of CNTs as a promising approach for enhancing the electrochemical performance and commercial viability of lithium-sulfur batteries.

1. Introduction

High theoretical capacity (1675 mAh kg^{-1}) and energy density (2600 Wh kg^{-1}) make Lithium-sulfur (Li–S) batteries a promising energy storage system for future technologies that surpass the performance of commonly commercial lithium-ion batteries (~300 Wh kg^{-1}) [1–6]. Therefore, high-energy batteries like Li–S batteries have a high potential for diverse applications, such as advanced electric-storage systems, Electronic gadgets, and high milage electric vehicles, which require high-energy density batteries as future demand increases [7–10]. The primary advantages of sulfur in lithium-sulfur (Li–S) batteries stem from its natural abundance, minimal environmental footprint, and cost-effectiveness [6,11–13]. Although lithium-sulfur (Li–S) batteries offer notable advantages, the commercial application still encounters the several limitations such as its insulating nature causing large polarization, solid-electrolyte interphase (SEI) layer formation, Li dendrite growth and notably, the shuttle effect caused by the dissolution of polysulfides [12, 14–16]. Due to its insulating nature, the low conductivity of sulfur and the poor contact between redox-active and conductive material hinder electron transfer in lithium-sulfur (Li–S) batteries. These problems are associated with the nonoptimal mixing of electrode

* Corresponding author.
** Corresponding author.
E-mail addresses: parkjw@keri.re.kr (J.-W. Park), ssunzero@keri.re.kr (H.-Y. Choi).
[1] These authors contributed equally to this work.

https://doi.org/10.1016/j.heliyon.2024.e35969
Received 3 May 2024; Received in revised form 6 August 2024; Accepted 7 August 2024
Available online 8 August 2024

materials and poor distribution of sulfur alongside conductive materials within the electrode [17]. Furthermore, the dissolution of polysulfides during the electrochemical reactions is influenced by the increase in sulfur content [18].

Commonly used conductive materials such as Super P and acetylene black struggle to address the deficiencies of Li–S batteries because they are constrained in facilitating electrochemical interactions between sulfur and conductive materials [19]. The unique morphology of multiwalled carbon nanotubes (MWCNTs) has recently garnered considerable attention, making them a promising conductive additive. This morphology not only enables high sulfur loading but also offers effective chemical and physical control over the polysulfide shuttling effect. However, their poor dispersibility in solvents is a major drawback that limits their sulfur loading [18,20,21]. To overcome this dispersibility problem, scientists have used different techniques such as surface treatment with chemical oxidants and metal doping [19–23].

Numerous techniques have been explored to address these challenges. Confining the active material with the conductive agent can prevent the shuttling effect and also strengthen the electrode structure [24–27]. Multiwalled carbon nanotubes (MWCNTs) have attracted many scientists due to their unique morphology for high sulfur loading and excellent conductivity properties which accelerate the reaction kinetics [17,28]. A significant drawback of MWCNTs is their poor dispersibility in solvents, which restricts their contact points with active materials and consequently limits the enhancement of sulfur loading [18,20]. These problems have been addressed by surface treatment such as chemical oxidation and doping of semimetals [21,24–26]. The Zhou group achieved a sulfur loading above 50 % into a 3D carbon nanotube (CNT) framework by integrating acid-treated carbon nanofibers as a sulfur host has a capacity decay rate of only about 0.024 percent per cycle over 500 cycles at a 2 C-rate [29]. A boron/oxygen co-doped porous carbon was synthesized by Wang et al. through an in-situ organic condensation reaction on the surface of CNTs, which exhibited the reversible capacity of 1077 mAh g^{-1} after 200 cycles at 0.2 C, with only 0.07 % decay per cycle [30]. However, these are complicated, multistep, and time-consuming processes.

In this work, we studied a simple and one-step surface modification of MWCNTs by comparing different acid functionalization treatments to enhance their dispersion and effect on the electrochemical performance. Acidic functionalization of the conductive material generates abundant-oxygen functional groups which play a vital role in enhancing the slurry dispersion. Among the various compositions evaluated using H_2SO_4, HNO_3, and H_2SO_4+HNO_3, the MWCNTs treated with a combination of HNO_3 and H_2SO_4 (SN-CNTs) in an 8:1:1 ratio exhibited superior cyclic performance compared to the other compositions. The functionalized SN-CNTs showed the minimum capacity decay of 0.29 % per cycle with a discharge capacity of 764 mAh g^{-1} at100th cycle with an average coulombic efficiency of 99 %.

2. Experimental

2.1. Preparation of functionalized MWCNTs

9.5 nm diameter multiwalled carbon nanotubes (MWCNTs), obtained from Nanocyl, Belgium were immersed in a concentrated HCl solution and magnetic stirred for 4 h to remove impurities. Subsequently, the MWCNTs were filtered, rinsed with deionized (DI) water multiple times until reaching a pH of approximately 7, and dried at 110 °C for 12 h.

To functionalize the multiwalled carbon nanotubes (MWCNTs), they were introduced into the solutions of H_2SO_4, HNO_3, and a mixture of H_2SO_4/HNO_3 (3:1, v/v), respectively. The mixtures were then stirred for 3 h at 80 °C. Afterward, the solutions were filtered, and the samples were washed several times with deionized (DI) water until the pH approached approximately 7. The obtained samples were dried at 110 °C for 12 h and named S-CNTs (H_2SO_4), N-CNTs (HNO_3), and SN-CNTs (H_2SO_4/HNO_3).

2.2. Preparation of the carbon-sulfur composite

The carbon-sulfur composite was prepared using a sulfur-melt strategy. First, 1.4 g of sulfur (Sigma Aldrich, 99.98 %) and 0.6 g of oxidized MWCNTs (S-CNTs, N-CNTs, and SN-CNTs) were added to ethanol and mixed via ball milling. The mixtures were filtered and dried at 50 °C for 12 h, followed by heating at 155 °C for 2 h in an inert (Ar) atmosphere; the mixtures were denoted as S-CNT@S, N-CNT@S, and SN-CNT@S.

2.3. Material characterization

Fourier-transform infrared spectroscopy (FT-IR) spectroscopy was conducted utilizing a VERTEX 80v Infrared Spectrometer from Bruker, USA. Raman spectra were acquired employing a Renishaw Raman spectrometer at a wavelength (λ) of 532 nm. The specific surface areas, pore sizes, and pore volumes were evaluated using the Brunauer–Emmett–Teller (BET) method via the BELSORP-max system with pre-degassing at 110 °C. X-ray diffraction (XRD) patterns were recorded using an X'Pert PRO instrument from Panalytical. Thermogravimetric analysis (TGA) was performed using a TGA Q600 instrument, employing a heating rate of 10 °C min-1 in an inert atmosphere. For the analysis of surface morphology and electrode slurry dispersion, field-emission scanning electron microscopy (FE-SEM) was utilized with an S-4800 instrument from Hitachi, coupled with energy-dispersive X-ray spectrometry (EDS).

2.4. Electrochemical measurements

Slurry coating technique with a doctor blade was used to fabricate the electrode by applying the dispersion onto 15-μm-thick aluminum foil, followed by vacuum drying at 50 °C for 12 h. The active material loading ranged from 0.7 to 1.0 mg cm^{-2}. Coin cells

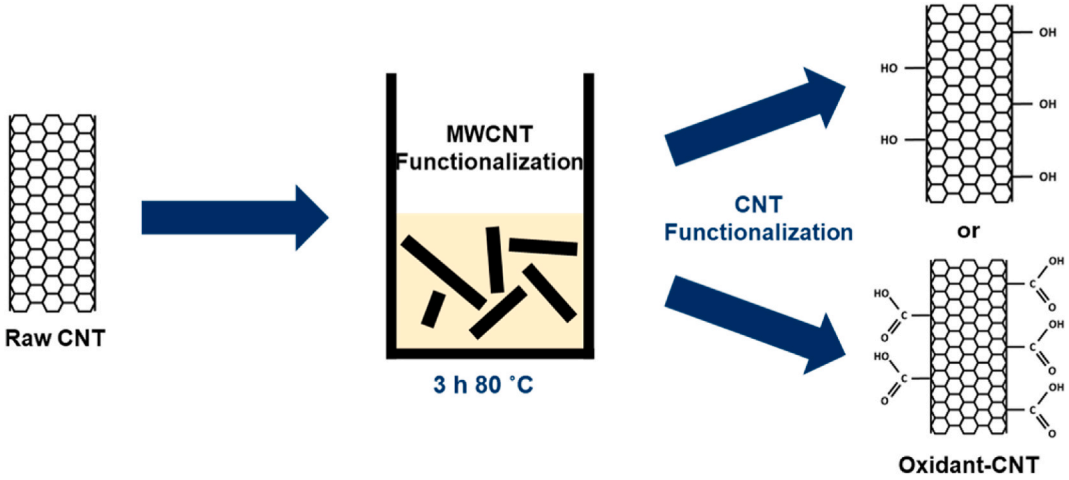

Fig. 1. Schematic diagram for the preparation of functionalized MWCNTs with various acids.

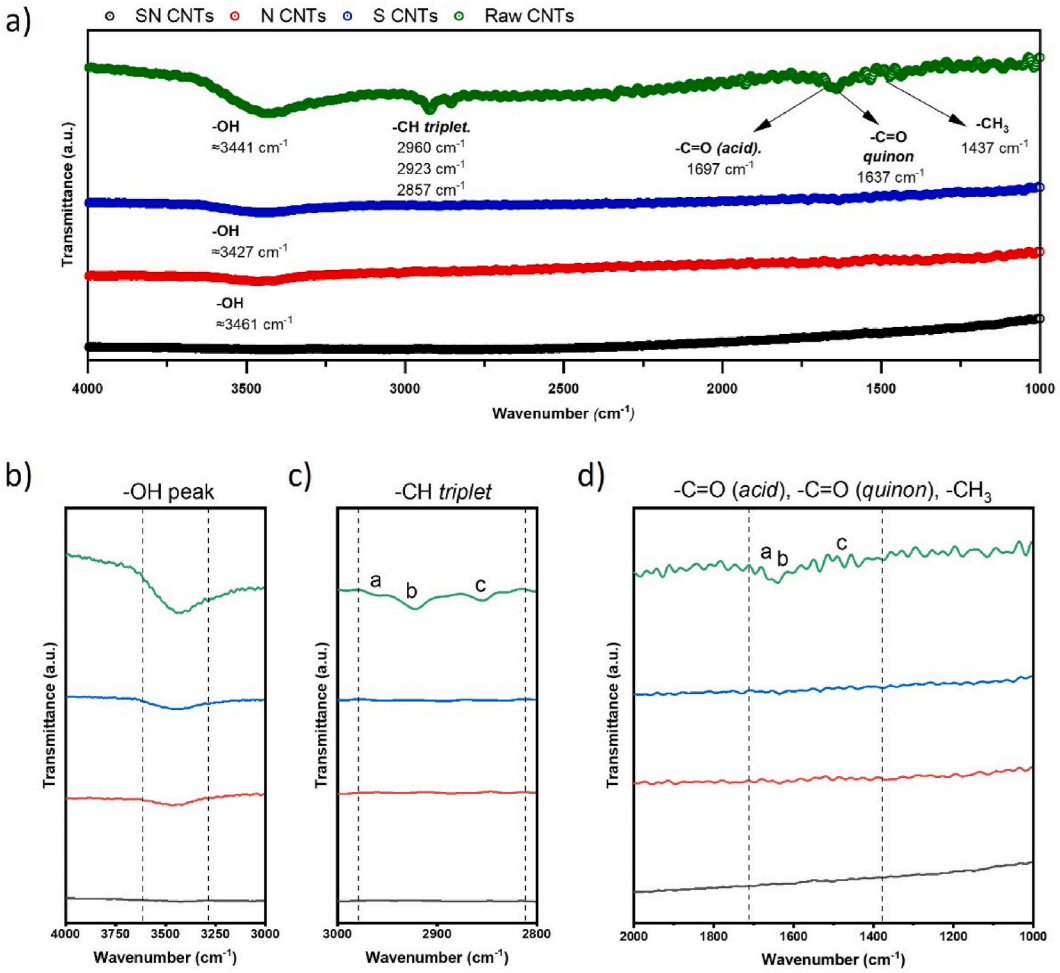

Fig. 2. (a) FT-IR spectra for raw CNTs, S-CNTs, N-CNTs, and SN-CNTs. (b) single Boand Spectra (c) Triple bond Spectra (d) double bond Spectra.

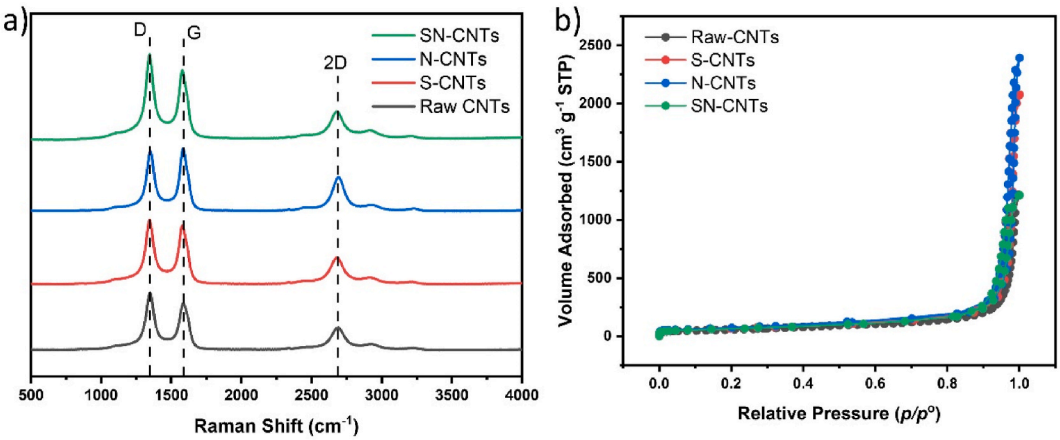

Fig. 3. (a) Raman spectra and (b) BET isotherms for raw and functionalized MWCNTs.

Table 1
Peak frequencies and Raman spectra assignments of raw and functionalized MWCNTs.

Sample	D band	G band	I_D/I_G	2D band
Raw CNTs	6711.7 (1347.6 cm^{-1})	5525.5 (1586.7 cm^{-1})	1.215	2867.6 (2691.2 cm^{-1})
S-CNTs	7659.8 (1344.1 cm^{-1})	7006.9 (1579.7 cm^{-1})	1.093	3482.7 (2682.1 cm^{-1})
N-CNTs	7011.9 (1351.2 cm^{-1})	7292.7 (1583.2 cm^{-1})	0.961	4106.1 (2691.2 cm^{-1})
SN-CNTs	10322.8 (1344.1 cm^{-1})	8596.5 (1579.7 cm^{-1})	1.201	4063 (2679.0 cm^{-1})

type CR 2032 were assembled in the glove box to investigate electrochemical performance. A 1 M solution of lithium bis(trifluoromethyl sulfonyl)imide was dissolved in a mixture 1,3-dioxolane and 1,2-dimethoxyethane in a volume ratio of 1:1 was used as electrolyte, additionally containing 1 wt% $LiNO_3$. A 500 μm thick Li-metal foil was used as a counter electrode with a commercially available polyethylene (PE) separator (SB16C) with a thickness of 16 μm. All electrochemical tests were performed using the Won-A Tech cycle tester within a voltage range of 1.5–3.0 V at a temperature of 25 °C. and capacity values are calculated based on the sulfur loading in each electrode.

3. Results and discussion

The acidic functionalization of MWCNTs is affected by many parameters, such as the process time, process temperature, and composition of the acidic solution. Previously, more attention was given to the processing time and high temperature required to functionalize the CNT surfaces. However, harsh conditions can cause structural damage. Particularly, Oxygen-containing functional groups, like carboxyl or hydroxyl groups, establish hydrophilic regions on the CNTs. These regions enable stronger hydrogen bonding with the surrounding water molecules. We functionalized MWCNTs by adding various acid solutions and stirring for 3 h at 80 °C. A schematic of this process is shown in Fig. 1. Fig. S1 shows the EIS spectra of functionalized MWCNTs show small semicircles as compared with raw CNT. The functionalization of MWCNTs not only enhanced the electronic conductivity between the CNTs and sulfur (Fig. S1) [31] but also helped to reduce polysulfide diffusion by chemical trapping [17].

Fig. 2a shows the FTIR spectra of raw MWCNTs and those functionalized with different acids. Raw CNT surface before acid treatment shows no evidence of functional groups, whereas S-CNTs, N-CNTs, and SN-CNTs show a broad peak at between 3427 and 3461 cm^{-1}(Fig. 2b), which can be assigned to the –OH stretching vibrations of the hydroxyl groups on the CNTs (COOH-CNTs). SN-CNTs show peaks at 1697, 1637, and 1437 cm^{-1} (Fig. 2d), which were assigned to the carboxylic acid, ester group C=O, and $–CH_3$ bending, respectively which indicates the strong effect of H_2SO_4 and HNO_3 mixture [32,33]. The –CH triple bond (Fig. 2c) and carboxylic characteristic peaks (Fig. 2d) are not intense enough to be clear in the spectrum in S-CNTs and N-CNTs. These results indicate that H_2SO_4/HNO_3 (3:1, v/v) was more effective for surface functionalization than H_2SO_4 or HNO_3.

In the Raman spectra of both raw CNTs and functionalized MWCNTs (as depicted in Fig. 3a), three distinctive peaks emerge at approximately 1340, 1580, and 2380 cm^{-1}, corresponding to the D band, G band, and 2D band, respectively, were observed. The intensities of the D and G bands represent the characteristics of the defect in-plane stretching vibrations of the C atoms [34]. The intensity ratios of these two bands (ID/IG) for the raw and functionalized MWCNTs were calculated and are presented in Table 1. The D/G ratios (ID/IG) of the raw CNTs, S-CNTs, N-CNTs, and SN-CNTs were 1.215, 1.093, 0.961, and 1.201, respectively. The D/G ratio of the SN-CNTs was higher than that of the S-CNTs and N-CNTs, indicating that the SN-CNTs have more structural defects and more oxidized sites on the CNT surface [35,36]. Fig. 3b shows the N_2 adsorption/desorption isotherms of raw and functionalized MWCNTs. All samples showed a similar type of isotherm (type III), and only a slight change in the surface area of the functionalized MWCNTs was observed, which indicates that the morphology of the MWCNTs was not affected by acid treatment. The surface areas (Fig. 3b) and pore

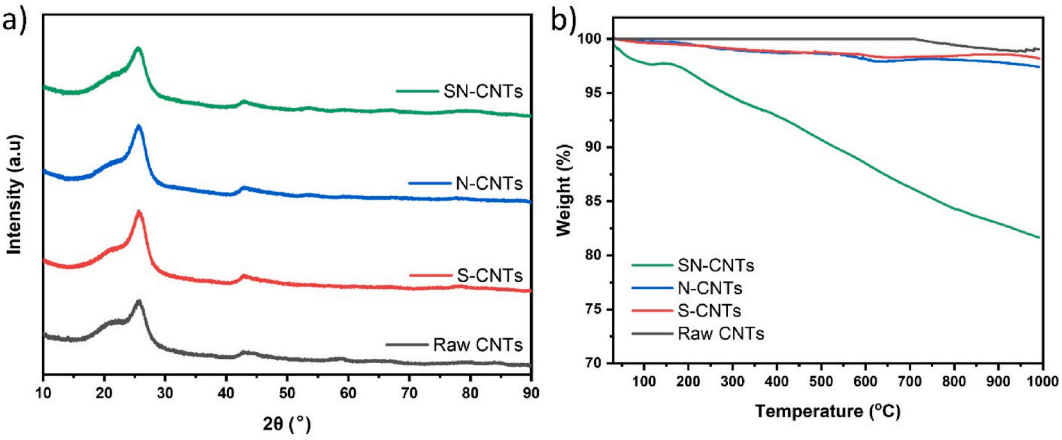

Fig. 4. (a) XRD patterns and (b) TGA curves of raw and functionalized MWCNTs.

volume (Fig. S2) of raw CNTs, S-CNTs, N-CNTs, and SN-CNTs were 200.49, 230.31, 262.02, 226.65 $m^2\ g^{-1}$ and 46.064, 52.914, 60.201, 52.074 $cm^3\ g^{-1}$, respectively. Table S1 summarizes the surface area, pore size, and pore volume of the raw and functionalized CNTs, which were calculated using the BET and Barrett-Joyner-Halenda (BJH) methods. This result indicates that minimum CNT structural damage occurred during acid treatment.

XRD was used to analyze the phase change caused by the acidic treatment of the MWCNTs. Fig. 4a reveals that there was no change in the XRD patterns of the raw and functionalized MWCNTs, confirming that the acid treatment of the MWCNTs did not affect the phase structure. Fig. S3a shows the XRD patterns of the MWCNTs@S with the incorporation of pure sulfur into the MWCNT structure. An α-sulfur crystal with an orthorhombic arrangement originating from cyclo-octa-sulfur (S_8) molecules was observed. Fig. S3a shows the seamless integration of the functionalized MWCNT peaks with the sulfur peak, providing compelling evidence that elemental sulfur was effectively impregnated into the structure of the functionalized MWCNTs. TGA was also performed to observe the functionalization of the MWCNTs by H_2SO_4, HNO_3, and H_2SO_4+HNO_3 treatments. In Fig. 4b, the weight losses of the raw and functionalized MWNCTs are shown by thermal analysis when they were heated to 1000 °C under an Ar atmosphere. As a result of the oxidative treatment, oxygen-containing functional groups were incorporated into the MWCNTs. Upon heating, these functional groups decomposed, leading to the release of CO and/or CO_2, depending on the specific groups attached [37,38]. The SN-CNTs exhibited a continuous weight loss as the temperature gradually increased until reaching 1000 °C, while raw CNTs, S-CNTs, and N-CNTs demonstrated nearly identical weight losses. For SN-CNTs, at temperatures above 150 °C, the functional groups began to decrease at a more pronounced rate, indicating a higher rate of weight loss. This demonstrates that the treatment involving H_2SO_4+HNO_3 introduced a greater number of functional groups than the other acid treatments. To determine the sulfur content of the MWCNT@S structure, TGA was conducted under oxidative conditions. Fig. S3b illustrates a notable weight loss, with the highest weight loss observed for SN-CNTs@S. A sharp decline in weight occurred from 133 to 323 °C. This weight loss was attributed to the desorption of sulfur and its subsequent chemical reaction to form SO_2 [26,39]. Consequently, the SN-CNTs@S structure exhibited a notably high total sulfur content compared to the other functionalized samples.

The dispersion properties of the raw and functionalized MWCNTs with sulfur were examined by SEM using a slurry-coated cathode, as shown in Fig. 5. The cathode slurry was prepared using a strongly adhering PAA binder, which also regulates the polysulfides by hydrogen bonding with the hydroxyl groups on the surface oxide layer of the Al current collector and –COOH groups of the PAA binder. Fig. 5a shows SEM images of the raw CNT electrodes, demonstrating an uneven dispersion of MWCNTs and sulfur because of the hydrophilic properties of the MWCNTs. In contrast, the electrode prepared with functionalized MWCNTs exhibited a uniform dispersion of sulfur and MWCNTs (Fig. 5b–d). Notably, SN-CNTs@S (Fig. 5d) displayed a more uniform coating without component cluster. This comparison highlights the influence of the extent of functionalization of the conductive material (MWCNTs) on the distribution of the material within the aqueous cathode slurry, with the sample treated with H_2SO_4+HNO_3 yielding the most favorable outcome.

To evaluate the electrochemical performance of the prepared cathodes, galvanostatic charge-discharge testing was conducted at a rate of 0.1 C. Fig. 6a shows the 2nd cycle galvanostatic charge-discharge curves of prepared cathodes, demonstrating the two typical plateaus of sulfur at approximately 2.3 and 2.1 V corresponding to the formation of long-chain (Li_2S_2, $4 < x \leq 8$) and short-chain (Li_2S_2/Li_2S), polysulfides, respectively [40–42]. The polarization of the SN-CNT cathode seemed to be alleviated compared to those of the other cathodes. The overpotential of the SN-CNTs was 240 mV, which was the smallest among the cathodes (300, 260, and 290 mV for raw CNTs, S-CNTs, and N-CNTs, respectively). This confirms that the functionalization of the carbon nanotube (CNT) surface and the uniform distribution of sulfur have enhanced the redox reaction kinetics of lithium polysulfides (LiPS) during the charge/-discharge process [17]. This improvement can also be attributed to the well-embedded structure of sulfur in SN-CNTs, which prevents the dissolution of sulfur in the electrolyte, facilitating the acquisition of electrons and thereby enhancing the reaction kinetics [42]. Furthermore, Fig. S4 shows the dQ/dV plot of SN-CNTs compared with raw CNTs. In the case of the SN-CNT sample, during the transition from S_8 to Li_2S, a broad, low peak was observed at 2.29V, and intense, sharp peaks were seen at 2.08V, 2.07V, and 2.04V.

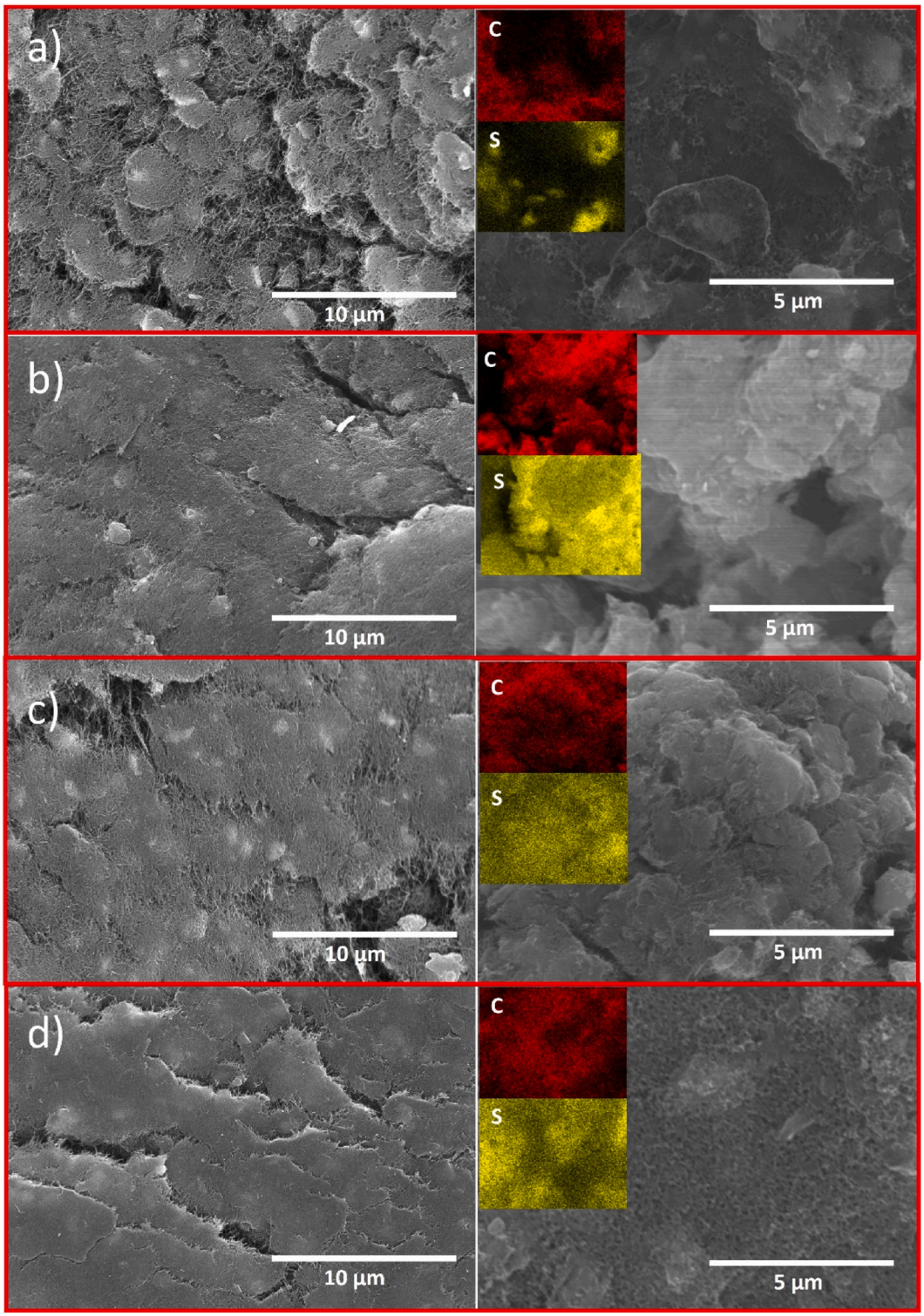

Fig. 5. SEM images of cathodes prepared with sulfur and functionalized MWCNTs. (a) Raw CNTs, (b) S-CNTs, (c) N-CNTs, and (d) SN-CNTs. The insets labeled "S" and "C" correspond to the signals from sulfur and carbon, respectively.

Conversely, for the raw-CNT sample, a similar peak appeared at 2.29V, but only a single sharp peak at 2.12V was observed in the low-voltage region. This difference can be attributed to the enhanced ion transport and more uniform sulfur distribution in the SNCNT sample, leading to multiple reaction pathways and more distinct electrochemical features compared to the raw-CNT sample [43]. The

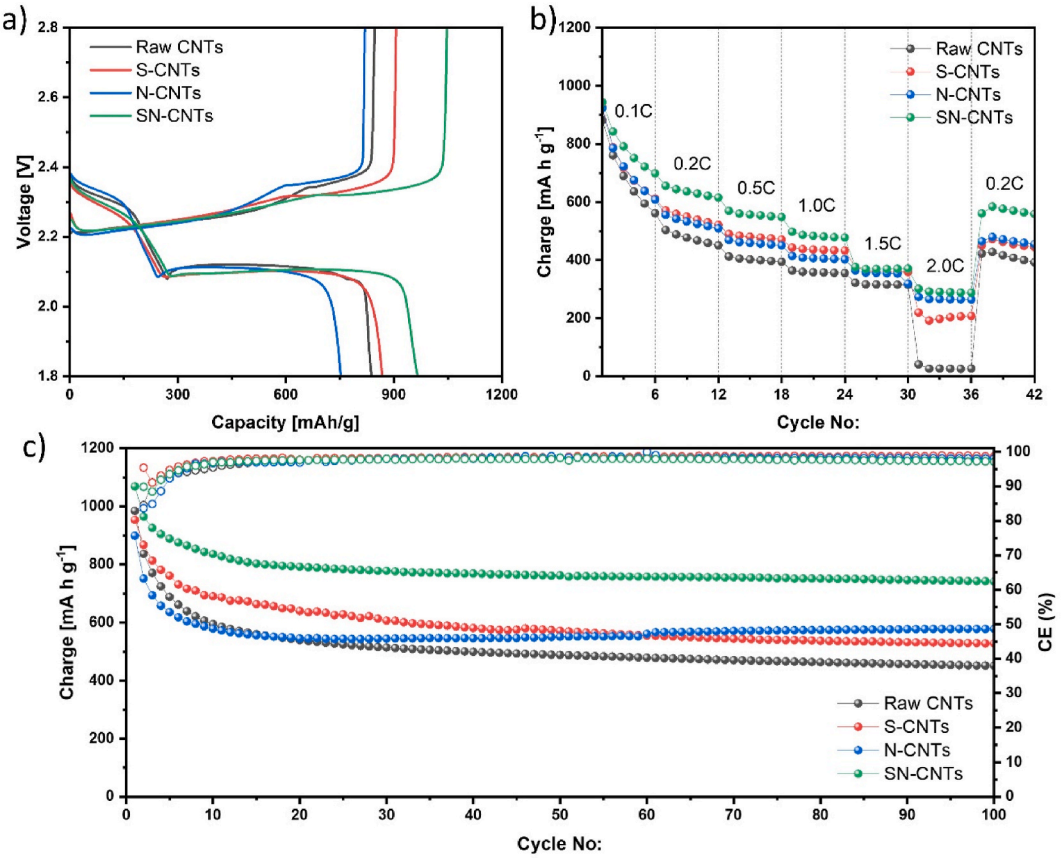

Fig. 6. Electrochemical testing for raw and functionalized MWCNTs: (a) galvanostatic charge-discharge, (b) C-rate, and (c) cycling test.

functional groups and defects in SN-CNTs provide more active sites for the sulfur reactions, resulting in sharper and more numerous peaks at lower voltages.

Additionally, during the $Li_2S \rightarrow S_8$ reaction, the SNCNT sample shows high-intensity peaks at 2.22V, 2.23V, and 2.32V, while the raw-CNT sample shows peaks at 2.22V and 2.24V similar to SNCNT but exhibits a high-shifted, relatively low-intensity peak at 2.34V. This can be explained by the better ion transport and more effective sulfur utilization in the SNCNT sample due to its functional groups and defects [35,36]. These characteristics lead to more efficient electrochemical reactions and higher peak intensities at specific voltages, whereas the raw-CNT sample shows less effective sulfur utilization and broader, less intense peaks.

The rate performance of the functionalized MWCNTs was also gauged at various current densities from 0.1 to 2 C, as shown in Fig. 6b. The discharge capacities of the raw CNTs, S-CNTs, N-CNTs, and SN-CNTs were 881, 927, 922, and 943 mA h g^{-1} at 0.1C, respectively. Among these cathodes, SN-CNTs showed superior rate capability and exhibited a discharge capacity of 301 mA h g^{-1} at 2 C, whereas the other cathodes showed lower capacities. When the current density was reset to 0.2 C, a reversible capacity of 561 mA h g^{-1} was produced by SN-CNTs, which is the highest among the electrodes, indicating the excellent stability of the electrode at various rates, whereas raw CNTs, S-CNTs, and N-CNTs produced 423, 451, and 464 mA h g^{-1}, respectively. Furthermore, the charge/discharge curves at different current densities are shown in Fig. S5 indicating the typical discharging platform of lithium-sulfur battery at high c-rate [44]. These results indicate that a well-functionalized and uniformly dispersed active material can enhance the performance of Li–S batteries.

The long cycling life span of the functionalized MWCNT electrodes was also evaluated at a C-rate of 0.5C for 100 cycles after the 10 precycles cycles at 0.1 C for sulfur activation, which required a long activation time, as shown in Fig. 6c [45]. SN-CNTs exhibited a specific charge/discharge capacity of 1075/1071 mA h g^{-1} with a coulombic efficiency of 100 %. After 100 cycles, the electrode retained a charge capacity of 764 mA h g^{-1}, corresponding to a capacity retention of 71 % with the capacity fade rate recorded at 0.29 % per cycle. In contrast, the raw CNT, N-CNT, and S-CNT electrodes exhibited slightly lower initial charge capacities of 991, 933, and 900 mAh g^{-1}, corresponding to initial coulombic efficiencies of 100, 98, and 100 %, respectively. After 100 cycles, raw CNT, N-CNT, and S-CNT electrodes exhibited the charge capacities of 460, 533, and 591 mAh g^{-1} corresponding to 46, 57, and 66 % capacity retention with higher capacity fade rates of 0.54, 0.43, and 0.34 % per cycle, respectively, indicating faster capacity degradation. The charging/discharging capacity of N-CNTs cathode is lower than that of Raw CNTs cathode this could be due to nitric acid introducing a high density of functional groups like carboxyl groups, creating more defects and increasing hydrophilicity. While this enhances interaction with sulfur and improves long-term stability, it also increases initial resistance, reducing electron transport efficiency

Table 2
Electrochemical properties of the previously reported oxidized CNTs electrodes for Li–S batteries and this work.

Electrode	S content (%)	Decay rate (%)	reference
Acidic oxidized CNTs	65	0.63 % @ 0.2 C	[48]
Pre-acid treatment + KOH activated CNTs	80	0.11 % @ 0.2 C	[49]
H_2O steam etched CNTs	78–89	0.19 % @ 0.2 C	[50]
Air-CNTs	70	0.31 % @ 0.2 C	[51]
CO_2-CNTs	80	0.17 % @ 0.2 C	[52]
Modified MWCNTs	40	0.20 % @ 0.5 C	[17]
Raw-CNTs	70	0.54 % @0.5 C	This work
S-CNTs	70	0.43 % @0.5 C	This work
N-CNTs	70	0.34 % @0.5 C	This work
SN-CNTs	70	0.29 % @0.5 C	This work

during the initial cycles, leading to lower initial discharge capacity compared to raw CNTs [46,47]. A comparison of the electrochemical results for long-term cyclic capability with other binders was also evaluated and is shown in Fig. S6; SN-CNTs showed better results with CMC and PVDF binders. A comparison of the capacity decay with those from other studies is summarized in Table 2.

Based on the aforementioned results, the utilization of functionalized MWCNTs positively influenced the electrochemical performance of Li–S cells. This favorable impact stems from the efficient electron conduction, rapid ion transport, heightened electrolyte retention, reinforced physical confinement of polysulfides (Fig. S7), and chemical attributes. The approach outlined in this study not only paves the way for the advancement of high-performance Li–S batteries with elevated sulfur loading but also holds promise for extension to other CNT-based energy storage systems.

4. Conclusion

In conclusion, this study demonstrates that functionalized MWCNTs, especially SN-CNTs, significantly enhance the electrochemical performance of Li–S cells. SN-CNTs show a reduced overpotential, superior rate capability, and excellent long-term stability compared to other cathodes. Further assessment of the rate performance at various current densities reinforced the superiority of the SN-CNTs, which displayed higher discharge capacities at both low and high rates. The remarkable stability of the electrode is evident in the long-term cycling tests at 0.5C for 100 cycles, with SN-CNTs maintaining a charge capacity of 764 mA h g^{-1}, corresponding to a capacity retention of 71 % and a minimal capacity fade rate of 0.29 % per cycle. These findings suggest that functionalization improves electron conduction, ion transport, electrolyte retention, and polysulfide confinement. This approach holds promise for advancing high-performance Li–S batteries and may be extended to other CNT-based energy storage systems.

CRediT authorship contribution statement

Gwang-Hun Kim: Methodology, Investigation, Data curation. **Asif Raza:** Writing – original draft, Data curation. **You-Jin Lee:** Funding acquisition, Data curation. **Doohun Kim:** Visualization, Resources. **Jun-Woo Park:** Resources. **Hae-Young Choi:** Writing – review & editing, Writing – original draft, Methodology, Investigation, Funding acquisition, Data curation.

Declaration of competing interest

The authors declare that they have no known competing financial interests or personal relationships that could have appeared to influence the work reported in this paper.

Acknowledgments

This work was funded by the Technological Innovation R&D Program (S3178742) from the Ministry of SMEs and Startups (MSS, Korea) and the Korea Electrotechnology Research Institute (KERI) primary research program through the National Research Council of Science & Technology (NST), supported by the Ministry of Science and ICT (MSIT) (Nos.24A01005).

Appendix A. Supplementary data

Supplementary data to this article can be found online at https://doi.org/10.1016/j.heliyon.2024.e35969.

References

[1] G. Li, S. Wang, Y. Zhang, M. Li, Z. Chen, J. Lu, Revisiting the role of polysulfides in lithium-sulfur batteries, Adv. Mater. 30 (2018) e1705590, https://doi.org/10.1002/adma.201705590.

[2] D. Lei, K. Shi, H. Ye, Z. Wan, Y. Wang, L. Shen, B. Li, Q. Yang, F. Kang, Y. He, Progress and perspective of solid-state lithium–sulfur batteries, Adv. Funct. Mater. 28 (2018) 1707570, https://doi.org/10.1002/adfm.201707570.

[3] R. Van Noorden, Sulphur back in vogue for batteries, Nature 498 (2013) 416–417, https://doi.org/10.1038/498416a.

[4] J. Liu, Z. Bao, Y. Cui, E.J. Dufek, J.B. Goodenough, P. Khalifah, Q. Li, B.Y. Liaw, P. Liu, A. Manthiram, Pathways for practical high-energy long-cycling lithium metal batteries, Nat. Energy 4 (2019) 180–186, https://doi.org/10.1038/s41560-019-0338-x.

[5] C. Xia, C.Y. Kwok, L.F. Nazar, A high-energy-density lithium-oxygen battery based on a reversible four-electron conversion to lithium oxide, Science 361 (2018) 777–781, https://doi.org/10.1126/science.aas9343.

[6] Z. Bai, Z. Wang, R. Li, Z. Wu, P. Feng, L. Zhao, T. Wang, W. Hou, Y. Bai, G. Wang, Engineering triple-phase interfaces enabled by layered double perovskite oxide for boosting polysulfide redox conversion, Nano Lett. 23 (2023) 4908–4915.

[7] J. Balach, T. Jaumann, M. Klose, S. Oswald, J. Eckert, L. Giebeler, Functional mesoporous carbon-coated separator for long-life, high-energy lithium–sulfur batteries, Adv. Funct. Mater. 25 (2015) 5285–5291, https://doi.org/10.1002/adfm.201502251.

[8] R.C. Longo, L.E. Camacho-Forero, P.B. Balbuena, Li2S growth on graphene: impact on the electrochemical performance of Li-S batteries, J. Chem. Phys. 152 (2020), https://doi.org/10.1063/1.5135304.

[9] B.P. Vinayan, Z. Zhao-Karger, T. Diemant, V.S.K. Chakravadhanula, N.I. Schwarzburger, M.A. Cambaz, R.J. Behm, C. Kübel, M. Fichtner, Performance study of magnesium–sulfur battery using a graphene based sulfur composite cathode electrode and a non-nucleophilic Mg electrolyte, Nanoscale 8 (2016) 3296–3306, https://doi.org/10.1039/C5NR04383B.

[10] R. Fang, C. Liang, Y. Xia, Z. Xiao, H. Huang, Y. Gan, J. Zhang, X. Tao, W. Zhang, Supercritical CO 2 mediated incorporation of sulfur into carbon matrix as cathode materials towards high-performance lithium–sulfur batteries, J. Mater. Chem. A. 6 (2018) 212–222, https://doi.org/10.1039/C7TA08768C.

[11] A. Manthiram, Y. Fu, S.-H. Chung, C. Zu, Y.-S. Su, Rechargeable lithium–sulfur batteries, Chem. Rev. 114 (2014) 11751–11787, https://doi.org/10.1021/cr500062v.

[12] T. Tao, S. Lu, Y. Fan, W. Lei, S. Huang, Y. Chen, Anode improvement in rechargeable lithium–sulfur batteries, Adv. Mater. 29 (2017) 1700542, https://doi.org/10.1002/adma.201700542.

[13] X. Hu, H. Jiang, X. Li, J. Mu, G. He, M. Yu, Flexible and conductive membrane with ultrahigh porosity and polysulfide-conversion catalytic activity for large-scale preparation of Li–S batteries, ACS Appl. Energy Mater. 6 (2022) 342–352.

[14] H. Wang, C. Xu, X. Du, G. Liu, W. Han, J. Li, Ordered porous metal oxide embedded dense carbon network design as high-performance interlayer for stable lithium-sulfur batteries, Chem. Eng. J. 471 (2023) 144338.

[15] J. Li, H. Li, J. Li, S. Yuan, M. Xiang, J. Guo, W. Bai, Z. Yang, Regulation of waste-derived hierarchically porous carbon for optimizing the sulfur cathode host of LiS batteries, J. Energy Storage 73 (2023) 109087.

[16] X. Lai, Q. Chen, H. Wang, C. Chen, Z. Chen, C. Chen, D. Sun, Metal-organic framework-derived heterostructural bi-phased Sm2O3 as a novel sulfur immobilizer for high-performance Lithium-sulfur batteries, J. Energy Storage 74 (2023) 109520.

[17] G.-H. Kim, Y.-J. Lee, J.-W. Park, A. Raza, M.B. Raza, D. Kim, M. Park, H. Choi, Enhanced performance of lithium-sulfur battery cathode via composition optimization using modified MWCNTs as a conductive material and poly (acrylic acid) as a binder, Int. J. Electrochem. Sci. (2023) 100217, https://doi.org/10.1016/j.ijoes.2023.100217.

[18] G. Yang, R. Tao, C.J. Jafta, C. Shen, S. Zhao, L. He, I. Belharouak, J. Nanda, Investigating multiscale spatial distribution of sulfur in a CNT scaffold and its impact on Li–S cell performance, J. Phys. Chem. C 125 (2021) 13146–13157, https://doi.org/10.1021/acs.jpcc.1c02288.

[19] M. Zheng, Y. Chi, Q. Hu, H. Tang, X. Jiang, L. Zhang, S. Zhang, H. Pang, Q. Xu, Carbon nanotube-based materials for lithium–sulfur batteries, J. Mater. Chem. A. 7 (2019) 17204–17241, https://doi.org/10.1039/C9TA05347.

[20] A. Gören, C.M. Costa, M.M. Silva, S. Lanceros-Méndez, State of the art and open questions on cathode preparation based on carbon coated lithium iron phosphate, Compos. Part B Eng. 83 (2015) 333–345, https://doi.org/10.1016/j.compositesb.2015.08.064.

[21] N.B. Saleh, L.D. Pfefferle, M. Elimelech, Aggregation kinetics of multiwalled carbon nanotubes in aquatic systems: measurements and environmental implications, Environ. Sci. Technol. 42 (2008) 7963–7969, https://doi.org/10.1021/es801251c.

[22] N. Wang, S. Pandit, L. Ye, M. Edwards, V. Mokkapati, M. Murugesan, V. Kuzmenko, C. Zhao, F. Westerlund, I. Mijakovic, Efficient surface modification of carbon nanotubes for fabricating high performance CNT based hybrid nanostructures, Carbon N. Y. 111 (2017) 402–410, https://doi.org/10.1016/j.carbon.2016.10.027.

[23] J.-W. Park, S.-C. Jo, M.-J. Kim, I.-H. Choi, B.G. Kim, Y.-J. Lee, H.-Y. Choi, S. Kang, T. Kim, K.-J. Baeg, Flexible high-energy-density lithium-sulfur batteries using nanocarbon-embedded fibrous sulfur cathodes and membrane separators, NPG Asia Mater. 13 (2021) 30, https://doi.org/10.1038/s41427-021-00295-y.

[24] P. Wang, X. Dai, P. Xu, S. Hu, X. Xiong, K. Zou, S. Guo, J. Sun, C. Zhang, Y. Liu, Hierarchical and lamellar porous carbon as interconnected sulfur host and polysulfide-proof interlayer for Li–S batteries, eScience 3 (2023) 100088.

[25] H. Liang, F. Tian, Z. Zeng, Y. Li, C. Wang, Two-Dimensional metal-free compounds of BC4N and BC6N2 with boron atoms as highly efficient catalytic centers toward sulfur redox in lithium-sulfur batteries, Appl. Surf. Sci. 606 (2022) 154773.

[26] X. Yan, Y. Li, X. Zhang, X. Zhao, B. Liu, Enhancing performance of NiCo Sulfide composite cathode by Mn doping in Li-S batteries, Electrochim. Acta 468 (2023) 143181.

[27] T. Li, Y. Li, J. Yang, Y. Deng, M. Wu, Q. Wang, R. Liu, B. Ge, X. Xie, J. Ma, In situ electrochemical activation derived LixMoOy nanorods as the multifunctional interlayer for fast kinetics Li-S batteries, Small 17 (2021) 2104613.

[28] Y. Dai, W. Zheng, X. Li, A. Liu, W. Zhang, X. Jiang, X. Wu, J. Tao, G. He, N-doped hierarchically porous CNT@ C membranes for accelerating polysulfide redox conversion for high-energy lithium–sulfur batteries, ACS Appl. Mater. Interfaces 13 (2021) 2521–2529.

[29] G.W. Sun, C.Y. Zhang, Z. Dai, M.J. Jin, Q.Y. Liu, J.L. Pan, Y.C. Wang, X.P. Gao, W. Lan, G.Z. Sun, Construction of all-carbon micro/nanoscale interconnected sulfur host for high-rate and ultra-stable lithium-sulfur batteries: role of oxygen-containing functional groups, J. Colloid Interface Sci. 608 (2022) 459–469, https://doi.org/10.1016/j.jcis.2021.09.144.

[30] X. Chen, Y. Xu, F. Du, Y. Wang, Covalent organic framework derived boron/oxygen codoped porous carbon on CNTs as an efficient sulfur host for lithium–sulfur batteries, Small Methods 3 (2019) 1900338, https://doi.org/10.1002/smtd.201900338.

[31] X. Cheng, W. Wang, A. Wang, K. Yuan, Z. Jin, Y. Yang, X. Zhao, Oxidized multiwall carbon nanotube modified separator for high performance lithium–sulfur batteries with high sulfur loading, RSC Adv. 6 (2016) 89972–89978.

[32] O.-K. Park, T. Jeevananda, N.H. Kim, S. Kim, J.H. Lee, Effects of surface modification on the dispersion and electrical conductivity of carbon nanotube/polyaniline composites, Scr. Mater. 60 (2009) 551–554.

[33] K.A. Worsley, I. Kalinina, E. Bekyarova, R.C. Haddon, Functionalization and dissolution of nitric acid treated single-walled carbon nanotubes, J. Am. Chem. Soc. 131 (2009) 18153–18158.

[34] Z. Lei, X. Chen, W. Sun, Y. Zhang, Y. Wang, Exfoliated triazine-based covalent organic nanosheets with multielectron redox for high-performance lithium organic batteries, Adv. Energy Mater. 9 (2019) 1801010.

[35] A.C. Ferrari, D.M. Basko, Raman spectroscopy as a versatile tool for studying the properties of graphene, Nat. Nanotechnol. 8 (2013) 235–246.

[36] J.S. Mehta, A.C. Faucett, A. Sharma, J.M. Mativetsky, How reliable are Raman spectroscopy measurements of graphene oxide? J. Phys. Chem. C 121 (2017) 16584–16591.

[37] A. Tomova, G. Gentile, A. Grozdanov, M. Errico, P. Paunović, M. Avella, A. Dimitrov, Functionalization and characterization of MWCNT produced by different methods, Acta Phys. Pol. A. 129 (2016) 405–408.

[38] J.L. Figueiredo, M.F.R. Pereira, M.M.A. Freitas, J.J.M. Orfao, Modification of the surface chemistry of activated carbons, Carbon N. Y. 37 (1999) 1379–1389.

[39] H. Cui, X. Yan, B. Liu, X. Zhao, X. Zhang, X. Zhao, X. Tong, Y. Wang, Y. Xing, Flower-like spherical Ni-benzimidazole derived Ni-NiO-C complexed with carbon nanotubes as electrocatalysts for lithium-sulfur battery, J. Alloys Compd. 931 (2023) 167402.

[40] C. Zhang, H. Bin Wu, C. Yuan, Z. Guo, X.W. Lou, Confining sulfur in double-shelled hollow carbon spheres for lithium–sulfur batteries, Angew. Chemie Int. Ed. 51 (2012) 9592–9595, https://doi.org/10.1002/anie.201205292.

[41] S. Zheng, Y. Chen, Y. Xu, F. Yi, Y. Zhu, Y. Liu, J. Yang, C. Wang, In situ formed lithium sulfide/microporous carbon cathodes for lithium-ion batteries, ACS Nano 7 (2013) 10995–11003, https://doi.org/10.1021/nn404601h.
[42] X. Cheng, W. Wang, A. Wang, K. Yuan, Z. Jin, Y. Yang, X. Zhao, Oxidized multiwall carbon nanotube modified separator for high performance lithium–sulfur batteries with high sulfur loading, RSC Adv. 6 (2016) 89972–89978, https://doi.org/10.1039/C6RA14581G.
[43] E. Peled, I. Shekhtman, T. Mukra, M. Goor, I. Belenkaya, D. Golodnitsky, Improving the durability and minimizing the polysulfide shuttle in the Li/S battery, J. Electrochem. Soc. 165 (2017) A6051.
[44] Q. Xiao, G. Li, M. Li, R. Liu, H. Li, P. Ren, Y. Dong, M. Feng, Z. Chen, Biomass-derived nitrogen-doped hierarchical porous carbon as efficient sulfur host for lithium–sulfur batteries, J. Energy Chem. 44 (2020) 61–67.
[45] B. Papandrea, X. Xu, Y. Xu, C.-Y. Chen, Z. Lin, G. Wang, Y. Luo, M. Liu, Y. Huang, L. Mai, Three-dimensional graphene framework with ultra-high sulfur content for a robust lithium–sulfur battery, Nano Res. 9 (2016) 240–248, https://doi.org/10.1007/s12274-016-1005-1.
[46] F. Avilés, J. V Cauich-Rodríguez, L. Moo-Tah, A. May-Pat, R. Vargas-Coronado, Evaluation of mild acid oxidation treatments for MWCNT functionalization, Carbon N. Y. 47 (2009) 2970–2975.
[47] L. Li, L.I. Feng, The effect of carbonyl, carboxyl and hydroxyl groups on the capacitance of carbon nanotubes, New Carbon Mater. 26 (2011) 224–228.
[48] W. Kong, L. Yan, Y. Luo, D. Wang, K. Jiang, Q. Li, S. Fan, J. Wang, Ultrathin MnO2/graphene oxide/carbon nanotube interlayer as efficient polysulfide-trapping shield for high-performance Li–S batteries, Adv. Funct. Mater. 27 (2017) 1606663.
[49] Y.C. Jeong, K. Lee, T. Kim, J.H. Kim, J. Park, Y.S. Cho, S.J. Yang, C.R. Park, Partially unzipped carbon nanotubes for high-rate and stable lithium–sulfur batteries, J. Mater. Chem. A. 4 (2016) 819–826.
[50] Z. Xiao, Z. Yang, H. Nie, Y. Lu, K. Yang, S. Huang, Porous carbon nanotubes etched by water steam for high-rate large-capacity lithium–sulfur batteries, J. Mater. Chem. A. 2 (2014) 8683–8689.
[51] L. Sun, D. Wang, Y. Luo, K. Wang, W. Kong, Y. Wu, L. Zhang, K. Jiang, Q. Li, Y. Zhang, Sulfur embedded in a mesoporous carbon nanotube network as a binder-free electrode for high-performance lithium–sulfur batteries, ACS Nano 10 (2016) 1300–1308.
[52] D. Wang, K. Wang, H. Wu, Y. Luo, L. Sun, Y. Zhao, J. Wang, L. Jia, K. Jiang, Q. Li, CO2 oxidation of carbon nanotubes for lithium-sulfur batteries with improved electrochemical performance, Carbon N. Y. 132 (2018) 370–379.